Asia-Pac. J. Atmos. Sci., 50(4), 497-506, 2014
DOI:10.1007/s13143-014-0039-0
pISSN 1976-7633 / eISSN 1976-7951

Stochastic Representation of Dynamic Model Tendency : Formulation and Preliminary Results

Myung-Seo Koo and Song-You Hong

Korea Institute of Atmospheric Prediction Systems, Seoul, Korea

(Manuscript received 8 January 2014; accepted 21 May 2014)

Abstract: Stochastic representation of forecast uncertainties has been taken into account to improve dynamical seasonal prediction. In this study, perturbing the dynamic tendency by a random number is introduced to account for inherent uncertainties associated with computational representations of the underlying partial differential equations that govern the atmospheric motion. Compared to the traditional approach to perturb the physical tendency, the sensitivity of fluctuations in forecast variables to the magnitude of random forcing is found to be greater in the case of perturbing the dynamical tendency. Realizing that the major advantage of stochastic tendency in traditional approaches lies in the increase in ensemble spread, our approach manifests a greater potential in the field of dynamical ensemble prediction. An evaluation of a simulated climate for a boreal summer demonstrates a significant enhancement in forecast skill in terms of the large-scale features and precipitation, when both the dynamical and physical tendencies are simultaneously perturbed. This finding implies that model uncertainties could be addressed in terms of not only the physical parameterization but also the dynamical portion that used to be regarded as deterministically solved.

Key words: Stochastic representation, model uncertainty, predictability, seasonal prediction

1. Introduction

Since predictability is highly sensitive to initial state (Lorenz, 1963, 1969), much attention has been paid to probabilistic forecasting in which an ensemble of varying initial conditions is run forward under the model to obtain an impression of the likely range of future states. Previous work has demonstrated that this ensemble forecasting method provides better reliability than a deterministic forecast in long-term projection (e.g., Molteni and Palmer, 1993; Richardson, 2000). However, the range of the projection given by the ensemble forecast could not properly cover the phase space of possible future states. Although in the field of data assimilation significant progress achieved in increasing the spread, for example singular vectors or bread vectors, the ensemble still remains under-dispersive and underestimates the true uncertainty of the atmospheric evolution (Buizza *et al.*, 2005; Bishop and Shanley, 2008).

Forecast error can be also attributed to model uncertainty, i.e. the inherent uncertainties associated with computational representations of the underlying partial differential equations that govern the atmospheric motion. This has resulted in the multi-model ensemble technique that samples uncertainty due to the differences in the model formulations and in the errors between the individual models. This technique has proven its outperformance in terms of ensemble spread and ensemble-mean error, compared to the traditional initial condition ensemble method (Krishnamurti *et al.*, 2003; Weigel *et al.*, 2008; Weisheimer *et al.*, 2011). Since model error might arise from a misrepresentation of physical processes on unresolved subgrid-scales, multi-physics (LaRow *et al.*, 2005; Kang and Hong, 2008; Ham and Hong, 2013) and multi-parameter (Murphy *et al.*, 2004; Stainforth *et al.*, 2005) schemes have also been used to attempt to account for model uncertainties due to physical parameterization in a single model framework. Recognizing the great uncertainty in the cumulus parameterization scheme among the physics modules in atmospheric models, Grell and Dévényi (2002) proposed a convective parameterization scheme that can use a large variety of closure assumptions in earlier formulations to generate a large spread in the solution. A similar approach was proposed by Krishnamurti and Sanjay (2003), which is based on the geographical distribution of performance for a particular cumulus parameterization scheme.

Another method is to stochastically represent model uncertainties by using a random number. Stochastically perturbed models provides the advantage of having all the ensemble members have the same climatology and model bias, in contrast to multi-model or multi-physics ensembles in which each ensemble member is actually a different model from its own dynamical attractor. Lorenz (1975) foresaw that the ultimate climate models will be stochastic; i.e., random numbers will appear somewhere in the time derivatives. This led to the development of a stochastic representation in parameterized physical tendency, known as the stochastic perturbed parameterization tendency (SPPT) scheme (Buizza *et al.*, 1999) (hereafter B1999). This SPPT scheme perturbs the total parameterized tendencies with a random number sampled from the uniform or Gaussian distribution with a spatial and temporal autocorrelation. Also, this SPPT scheme was found to improve the skill of the probabilistic prediction in terms of the

Corresponding Author: Song-You Hong, Korea Institute of Atmospheric Prediction Systems, 4F, Hankuk Computer Building, 35 Boramae-ro 5 gil, Dongjak-gu, Seoul 156-849, Korea.
E-mail: songyouhong@gmail.com

ensemble spread in a medium-range forecast (Palmer *et al.*, 2009; Weisheimer *et al.*, 2011). It is noted that major benefits of the SPPT scheme include the improvement in probabilistic forecast skill, especially in terms of ensemble spread.

Recently it is recognized that uncertainties in the dynamical component of the forecast model also need to be addressed. The upscale cascade of energy from either sub-grid scales or scales that are poorly resolved in the model, is thought to be a source of model error, and considerable effort has been put into formulating a stochastic kinetic energy backscatter (SKEB) scheme (Shutts, 2005; Berner *et al.*, 2009). This scheme outperformed a multi-physics scheme (Berner *et al.*, 2011) and the SPPT scheme (Jung *et al.*, 2005) in terms of mesoscale ensemble prediction. In addition to the numerical energy cascade error, several grid-scale model errors exist due to the approximated governing equation itself and other components of the model formulations such as the truncation error (e.g., Teixeira *et al.*, 2007; Romps, 2012a, b). On the other hand, Hong *et al.* (2013a) demonstrated that there is another uncertainty for weather and climate models that could produce different results on computing platforms with different software system, despite using the same code.

Although past resolution increases have been providing continuously better forecasts especially in the short forecast range, Buizza (2010) and Berner *et al.* (2012) suggested that simple resolution increases without model improvements or the stochastic representation of model uncertainty would incur limited improvements in the long forecast range in the future. In this context, we argue that physical parameterizations may be more of an "*unknown*" problem than an "*uncertain*" issue at present. This means that understanding the physical processes is necessary to revise these issues that are still unsolved. Besides, some sub-grid scale formulation in parameterized physical processes would disappear at cloud-resolving scale resolutions, as computer resources develop, leading to a reduction in unknown processes, for example, the cumulus parameterization scheme in atmospheric models (Tao *et al.*, 2003). The cut-off grid spacing for each of physics component was discussed in Hong and Dudhia (2012).

The purpose of this study is to investigate the effects of stochastic perturbation of the dynamical model tendency, which has not been attempted so far, on the predictability of the seasonal ensemble prediction. The paper is organized in following manner. In the next section, the stochastic forcing configuration is described. In section 3, we discuss the sensitivity to random perturbation, and in section 4, its impact on the seasonal ensemble prediction. A summary and discussion are given in the final section.

2. Stochastic forcing configuration

For any component of the state vector (χ), the model equation can be defined as:

$$\frac{\partial \chi}{\partial t} = D + P, \tag{1}$$

where t is the time, and D and P designate the dynamical and physical tendencies, respectively. The horizontal diffusion term is assumed to be part of the dynamical component. Random perturbing is applied to the tendency after all of the dynamical and physical forcings are computed. Modulation of dynamic tendency is also computed on grid point space to easily visualize the evolution of tendency. For three-time-level semi-implicit integration, the model tendencies are perturbed as shown below:

$$D'_j = \langle r_j \rangle_\chi \left[\frac{\chi_j^+ - \chi_j^{n-1}}{2\Delta t} \right], \tag{2a}$$

$$P'_j = \langle r_j \rangle_\chi \left[\frac{\chi_j^{n+1} - \chi_j^+}{2\Delta t} \right], \tag{2b}$$

$$T'_j = \langle r_j \rangle_\chi \left[\frac{\chi_j^{n+1} - \chi_j^{n-1}}{2\Delta t} \right], \tag{2c}$$

where $^+$ indicates the provisional solution of the dynamical process, $'$ designates the perturbed tendency, $\langle r_j \rangle_\chi$ is the random number for variable χ at the j-grid point, and T designates the total tendency in a given time step, from time $n-1$ to time $n+1$.

A different random forcing is applied at every grid point without the consideration of the spatial correlation in both horizontal and vertical directions, but the impact of the spatial correlation on kinetic energy (KE) will be briefly discussed in section 3. Random numbers are sampled uniformly by the Fortran intrinsic function. This sampling method depends on the initial forecast time only, so stochastically-perturbed integrations yield the same results as long as the initial conditions are identical. The magnitude of stochastic forcing can be controlled by the interval (I) with 1 as the center. For example, if I is 1.0, then $\langle r_j \rangle_\chi$ ranges between 0.5 and 1.5. The maximum interval for preserving the vector direction is 2.0, ranging between 0.0 and 2.0.

B1999 stated that the sort of random error that occurs in parameterized forcing will be coherent between the different parameterization modules and will have a certain coherence on the space- and time-scales associated with, for example, the organized convection schemes. The notion of coherence among modules allows the stochastic perturbation to be based on the total tendency from all of the parameterized processes rather than on the parameterized tendencies from each of the individual modules. Based on this concept, the total physical tendency is used to perturb the parameterized tendencies as presented in Eq. (2b).

Bearing in mind that the predictability decreases along with the forecast time and that the KE sensitivity, due to random forcing, increases along with height (see Section 3 for more details), we suggest a stochastic forcing configuration that is dependent on both the forecast time and vertical layer as shown below:

$$I(\eta, t) = \begin{cases} I_{\max} e^{\eta - 1} e^{\frac{t - t_r}{3}} & t \le t_r \\ I_{\max} e^{\eta - 1} & otherwise \end{cases}, \tag{3}$$

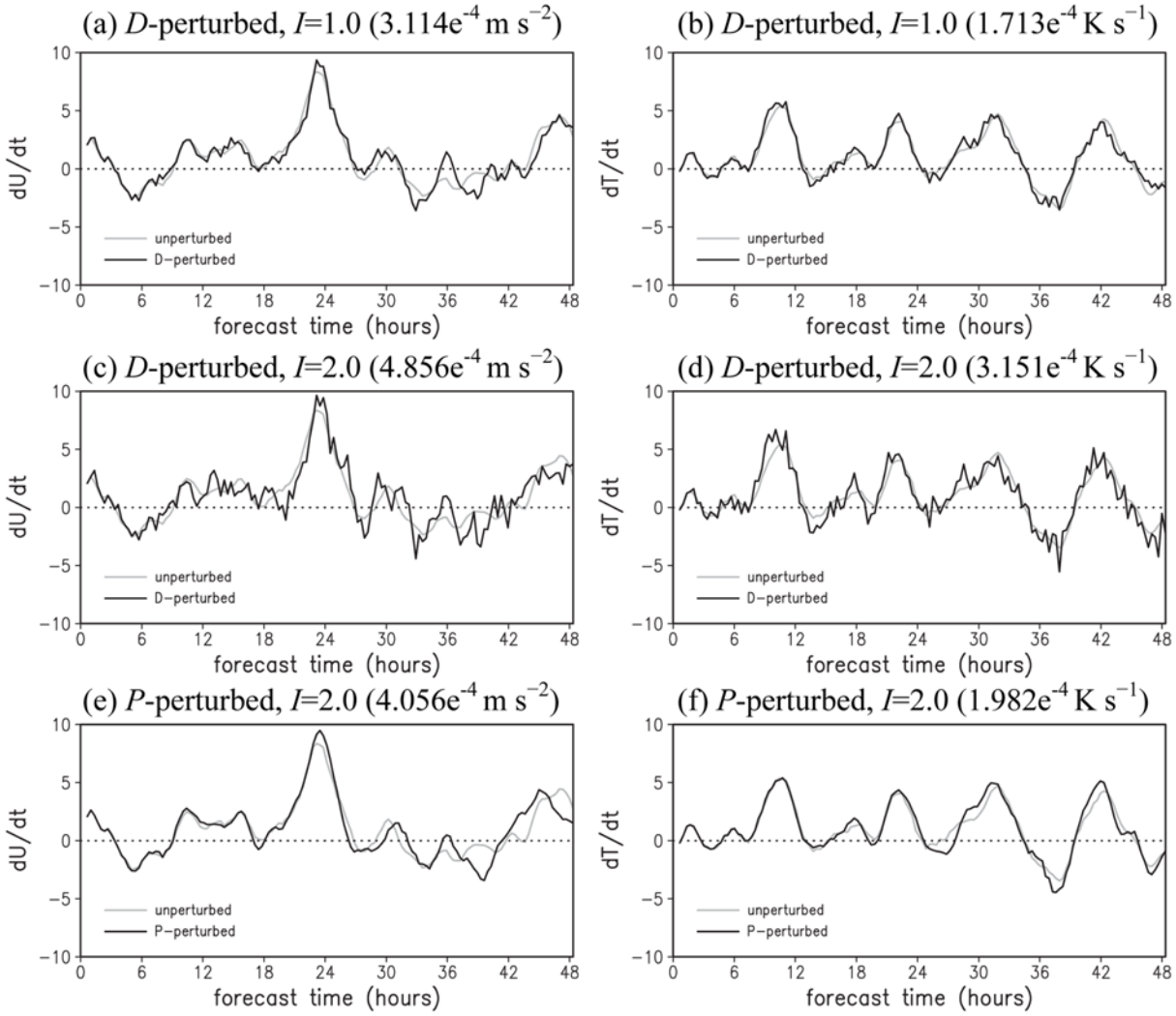

Fig. 1. Time series of the unperturbed (gray) and perturbed (black) total tendencies for (left) zonal wind (m s^{-2}) and (right) temperature (K s^{-1}) at 700-hPa averaged over a trough and light precipitation region (115-125°E; 35-45°N) during the first 48-hour forecasts at a T62L28 resolution, which are normalized by the averaged value (parenthesis) calculated from the unperturbed tendency. Dynamical tendencies are perturbed on the intervals of (a-b) 1.0 and (c-d) 2.0, and while the (e-f) physical tendencies are perturbed on the interval of 2.0.

where I_{max} is the maximum interval at a reference time (t_r) in the day, and η is the generalized vertical coordinate. Stochastic forcing exponentially decreases upwards and increases along with the forecast time until t_r-day, while the random interval does not change after t_r-day.

The impact of temporal correlation is additionally investigated because the configurations, in which the random forcing is changed every time step, have a small impact on the ensemble spread (see B1999), and such frequent sampling would impose a significant computational burden. We conducted a sensitivity test for the temporal correlation at a T254L64 (254 truncated total wavenumber, approximately 50 km in the horizontal; 64 vertical layers) resolution; random numbers are updated every time step (120 seconds), every 3 hours, and every 6 hours but fixed for each period. The results were not sensitive to the sampling time intervals less than 3 hours, while the 6-hourly random sampling yielded slightly different results (not shown).

3. Sensitivity to the magnitude of random forcing

In this section, stochastic forcing is designed through a sensitivity test to determine the size of the perturbations.

The model used is the Global/Regional Integrated Model system (GRIMs) (Hong *et al.*, 2013b), a multi-scale atmospheric modeling system with unified physics, which has been created for use in numerical weather prediction, seasonal simulations, and climate researches, on a global to regional scale. The selected dynamical core and physics package are the spherical harmonics and GRIMs version 3.1, respectively, and Hong *et al.* (2013b) contains further details. The initial conditions are taken from the National Centers for Environmental Prediction

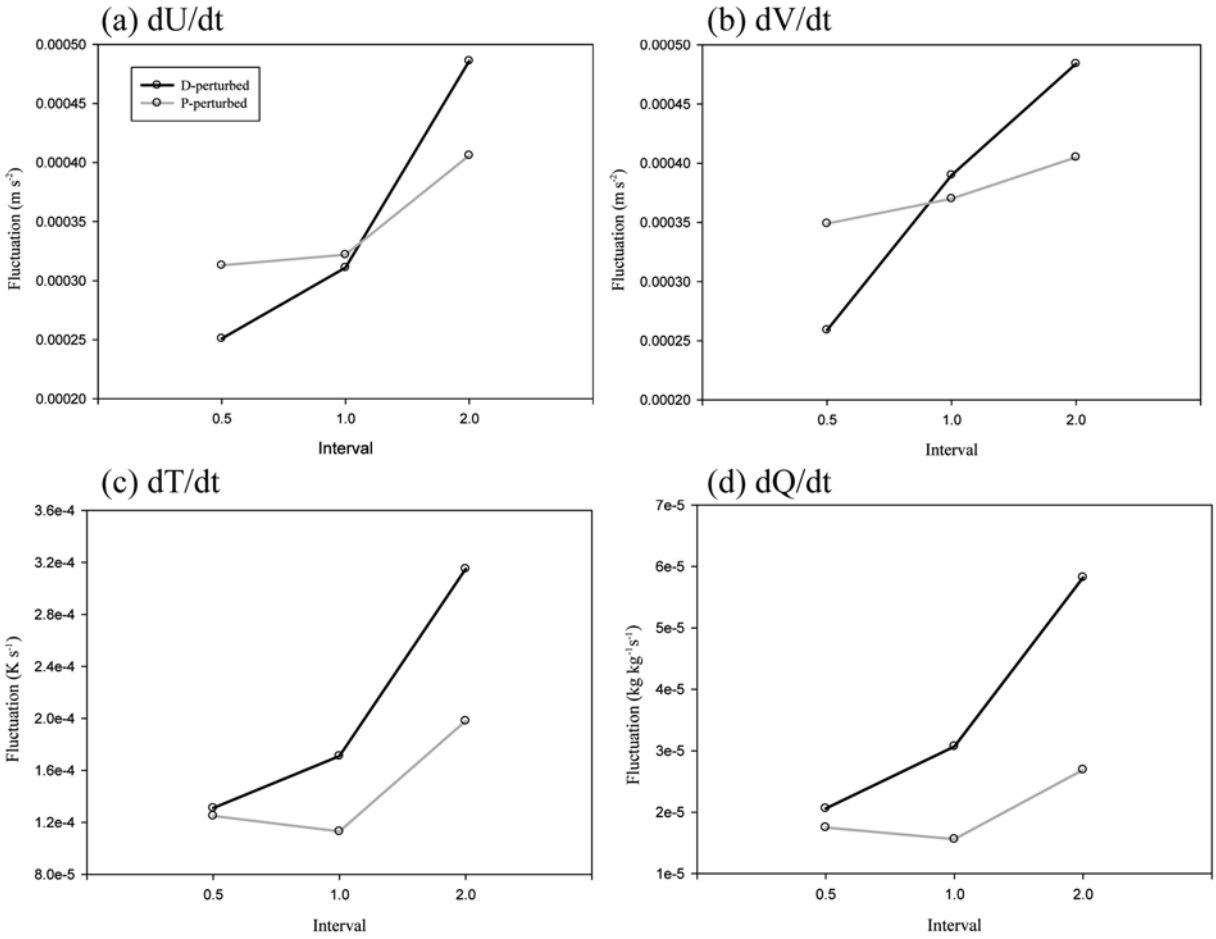

Fig. 2. Fluctuation magnitude of the perturbed total tendencies in (a) zonal wind (m s^{-2}), (b) meridional winds (m s^{-2}), (c) temperature (K s^{-1}), and (d) specific humidity (kg kg^{-1} s^{-1}) at 700 hPa, when perturbation is applied to the dynamical (black) and physical (gray) tendencies with the intervals of 0.5, 1.0, and 2.0.

(NCEP) Global Forecast Model (GFS) final analysis data at T574L64 resolution.

The impact of the stochastic forcing on the model tendencies is investigated, using a single deterministic forecast starting at 0000 UTC 14 July 2001. Three 10-degree square regions characterized by very different weather conditions are selected similar to B1999. The averaged values of the unperturbed and perturbed tendencies are compared for the first 48-hour forecast. Figure 1 shows the time series of the total tendencies of the zonal wind and temperature at 700 hPa for the region with a trough and light precipitation (115°E-125°E; 35°N-45°N), simulated from the unperturbed and perturbed simulations at a T62 resolution (approximately 200 km in the horizontal). The total tendencies are normalized by the time averaged value of the unperturbed total tendency. In general, the variation of total tendencies does not significantly differ between the unperturbed and perturbed integrations for the zonal wind and temperature (Fig. 1), as well as the meridional wind and specific humidity (not shown), with the exception of some fluctuation in the perturbed tendencies. For the case of smaller intervals (I = 0.1, 0.2, and 0.5), the fluctuations become weaker (not shown). These features are common among other regions, including the Pacific region with anticyclone (160°W-150°W; 35°N-45°N) and the tropics region with intense precipitation (130°E-140°E; 0°-10°N) (not shown). When the forcing interval is doubled in the dynamical tendency (i.e., I = 2.0), the perturbed total tendencies are more variable in comparison to those with I = 1.0 (cf. Figs. 1a, b and 1c, d). However, the variation is less sensitive to the size of the perturbation in the physical tendency (Figs. 1e, f). Despite the strong interval of 2.0, the total tendencies do not fluctuate as much as the tendencies caused by perturbing the dynamical tendency (cf. Figs. 1c, d). This result is expected, because the magnitude of the dynamical tendency is generally greater than that of the physical tendency, except near the surface.

Figure 2 clearly shows the difference in the sensitivity to the random forcing interval for the dynamical and physical tendencies at 700 hPa. The fluctuation magnitude is defined as the root-mean-squared difference between the perturbed and unperturbed total tendencies during the 48-hour forecast. As the interval becomes higher, the perturbed total tendency fluctuates more noticeably in both cases, but the sensitivity is

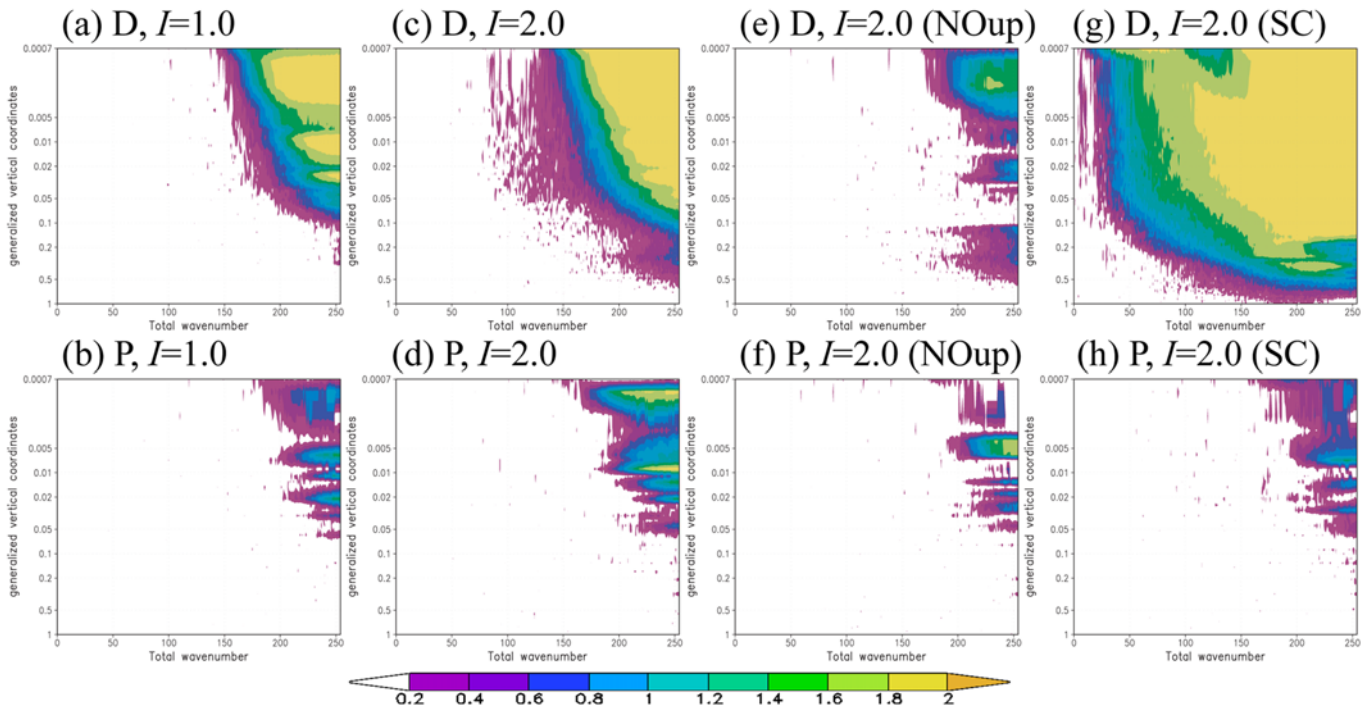

Fig. 3. Normalized absolute difference in the total kinetic energy spectrum between the unperturbed and perturbed simulations at a T254L64 resolution. The (upper panels) dynamical (D) and (lower panels) physical (P) tendencies are perturbed on the intervals of (a-b) 1.0 and (c-f) 2.0. In (e-f), random perturbation is not applied to the upper layer above 0.1 (NOup). In (g,h), random perturbation is identically applied every 10-degree spacing for spatial correlation (SC).

quite weak for the physical tendency when compared to the dynamical tendency. In addition, the temperature and specific humidity fluctuate less at $I = 1.0$ than at $I = 0.5$ for the physical tendency, despite the belief about the larger the tendency fluctuation, the greater the perturbation magnitude. The reduced fluctuation at $I = 1.0$ compared to that at $I = 0.5$ seems to be due to the fact that the adjustment between mass and winds optimally reduces modulated mass fields by the random forcing on physical tendency. Dynamic tendency fluctuation increases as the random forcing is strengthened because its sensitivity is much larger than that of the physics tendency fluctuation, so that adjustment between mass and winds could be relatively small. Sensitivity test at a T126 resolution (approximately 100 km) yielded the same conclusion as in Figs. 1 and 2 (not shown).

The perturbation in both the dynamical and physical tendencies should not be excessive in terms of KE ($m\ s^{-2}$) spectrum. Experiments at higher resolution at a T254 (approximately 50 km) are designed to examine the KE at small scales. For 200-hPa KE spectrum, the perturbation in both the dynamical and physical tendencies did not significantly deteriorate the KE spectrum distribution of unperturbed simulation (Figures not shown). To find out how sensitive the KE is to random perturbation in detail, we define the normalized absolute difference in KE (dimensionless) as

$$KE_{diff} = \frac{|KE' - KE|}{0.5(KE' + KE)}, \quad (4)$$

which ranges from 0 to 2. In Fig. 3, this KE difference is examined at all vertical layers. The KE is sensitive to the perturbation size in the dynamical tendency (cf. Figs. 3a, c) more than that in the physical tendency (cf. Figs. 3b, d), which is consistent with the tendency sensitivity. In addition, the amplitude of KE difference increases with the vertical layer for both of the tendency perturbations. Large dynamical tendencies in the upper layers are likely to be related to jet stream, which should not have the same uncertainty associated with them as those in the lower troposphere.

It is plausible that the increase of KE in the upper layer is caused by the upward transport of unphysical gravity wave generated in the lower layer. To check this out, we further examine the impact of restricting the stochastic perturbation in the upper layer between $\eta = 0$ and 0.1. In Figs. 3e, f, the upward transport of unphysical gravity waves seems to play a role for the both perturbations to dynamical and physical tendencies. This indicates that the unphysical gravity waves might pay a major contribution to the kinetic energy difference. B1999 used a 10-degree spatial and 6-hour temporal autocorrelations, which are comparable with the Rossby deformation radius and twice the Coriolis time-scale ($1/f$, where f being the Coriolis parameter) in middle latitude. Shutts (2005) stated that smaller correlation-scales tend to generate high-frequency gravity waves whose impact on weather system evolution is only slight. When introducing 10-degree spatial correlation in the random pattern, the deposition of upward

propagating energy is somewhat remedied for the physical tendency perturbation (Fig. 3h), whereas not at all for the dynamical tendency perturbation, rather aggravated (Fig. 3g).

An additional test was carried out in order to examine the impact of the random forcing whose magnitude varies with height from the ground. When the magnitude of random forcing was identically applied to all of the vertical layers, there was less discernible improvement in forecast skill. Therefore, the perturbation magnitude varying with height from the ground might be suitable in terms of not only the model stability, but also the forecast skill.

The above finding implies that the consideration of spatial correlation provides the antithetical impact on the KE spectrum for the dynamical and physical tendencies. It is assumable that larger (smaller) correlation-scales generate lower (higher) frequency waves, which means that spatial correlation can affect large-scale dynamics. Since the magnitude of dynamical tendency is generally greater than that of physical tendency, except near the surface, the effect of spatial correlation in physics perturbation on large-scale dynamics might be less than that in dynamics perturbation. Our main focus here is to examine the impact of stochastic perturbation in dynamics compared to that in physical parameterization, thus we do not consider spatial correlation in this study. Elaborating the random forcing while considering the spatial correlation could be attempted in future, depending on the robust evaluation of the forecast skill for weather and climate.

4. Seasonal simulation

Seasonal simulations are performed at a resolution of T126L64 (approximately 100 km in the horizontal). The initial conditions are taken from the NCEP-Department of Energy (DOE) Atmospheric Model Intercomparison Projection (AMIP) II reanalysis (RA2, Kanamitsu *et al.*, 2002), and the observed sea surface temperature (SST) is updated daily from the optimal interpolation SST weekly data set (Reynolds and Smith, 1994). To avoid introducing uncertainties from the initial data on a seasonal forecast time scale, ten-member ensemble runs for each experiment, with a one-day interval, are performed with an approximate 4-week lead-time for a boreal summer of June-July-August in 1996, in which the SST over the equatorial Pacific is close to a seasonal climatology.

Table 1 summarizes the experimental setup to examine the impact on the seasonal ensemble prediction. For stochastic runs perturbing the dynamical tendency (DYN, Eq. 2a) and the physical tendency (PHY, Eq. 2b), random numbers are sampled using Eq. (3) with $I_{max} = 2.0$ and $t_r = 10$-day at every three hour. The combination set of the DYN and PHY is also configured as DPT, i.e., perturbing dynamical and physical tendencies simultaneously. The experiment of perturbing the total tendency (i.e., Eq. 2c) is not addressed in this section, since its result is quite similar to the DYN's result, which is probably caused by the comparable magnitude between the dynamical and total tendencies.

Table 1. Experimental setup for unperturbed (CTL) and stochastically-perturbed dynamical (DYN) and physical (PHY) tendencies. The DPT indicates the combination of DYN and PHY. Stochastic forcing exponentially increases with forecast time up to 10 day (t_r; reference time), at which the maximum interval (I_{max}) is 2.0, and exponentially decreases with vertical layer. Random numbers are updated at every three hour.

Experiment	Perturbed tendency	I_{max}	t_r
CTL	-	-	-
DYN	Dynamical tendency	2.0	10-day
PHY	Physical tendency	2.0	10-day
DPT	DYN + PHY	2.0	10-day

Zonal mean, standing eddy, and transient eddy of the 500-hPa geotential height are decomposed to investigate the impact on the meridional circulation (three-cell circulation), stationary planetary waves (wavenumber 1-3 eddies), and weather systems (mid-latitude cyclones and anticyclones), respectively, which are calculated as

$$\Phi = [\overline{\Phi}] + \overline{\Phi}^* + \Phi', \tag{5}$$

where Φ is the daily mean geopotential height; overbar and bracket indicate 3-month time and zonal averages, respectively; $'$ and * indicate the eddies from the 3-month time and zonal averages, respectively. Although the patterns of zonal mean ($[\overline{\Phi}]$) and transient eddy (Φ') are almost the same among the three perturbed and unperturbed runs (not shown), the skill scores (spatial correlation/root-mean-squared error) for the simulated standing eddy ($\overline{\Phi}^*$), compared to the RA2 data, are as follows: in descending order, DPT (0.710/23.43), DYN (0.684/24.38), CTL (0.667/25.09), and PHY (0.661/25.28) (Fig. 4).

Figure 5 shows the analysis for the transient eddy momentum flux ($u'v'$; $m^2 s^{-2}$) to elucidate the characteristics of poleward eddy flux. Compared to the RA2 (Fig. 5a), the CTL run tends to strengthen the three jet cores of the mid-latitudes but weakened the easterly wind at the upper layer in the southern hemisphere (Fig. 5b). The DYN run moderately reduces the bias in the cores (Fig. 5c), while the PHY run shows positive impact on the upper layer in the southern hemisphere (Fig. 5d). Interestingly, most of the biases of the CTL run are quite well corrected by the DPT run when compared to the DYN and PHY runs (Fig. 5e). This positive impact on poleward transport also appears in the transient eddy heat flux ($v't'$; not shown).

Figure 6 and Table 2 show the seasonal precipitation pattern and its statistical verification scores, respectively, compared to the Climate Prediction Center (CPC) Merged Analysis of Precipitation (CMAP, Xie and Arkin, 1997) data. It is clear that the CTL run satisfactorily reproduces the tropical rainfall comparable to the observations of the main rain-belt along the Intertropical Convergence Zone (ITCZ) over the Pacific and Atlantic, albeit with exaggerated precipitation in terms of global mean (2.71 versus 3.43 mm d^{-1}) and double ITCZ (Fig.

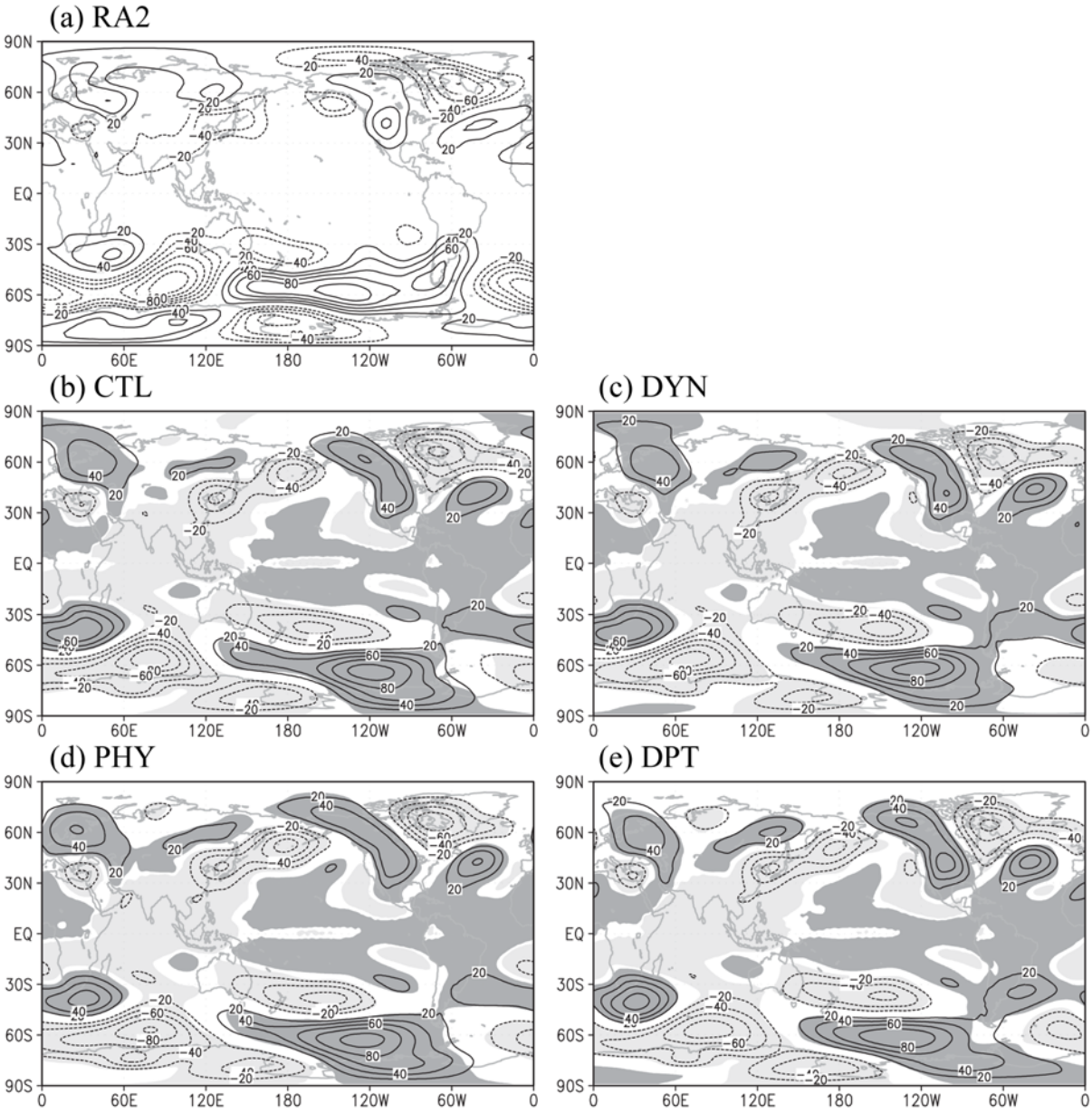

Fig. 4. Standing eddy of the 500-hPa geopotential height (m) for a boreal summer of June-July-August in 1996, obtained from the (a) RA2 data and simulated from the (b) CTL, (c) DYN, (d) PHY, and (e) DPT runs at a T126L64 resolution.

6), which is a deficiency that has been commonly observed among many general circulation models (Covey *et al.*, 2003; Dai, 2006). Compared to the CTL run, the DYN and PHY runs produce more precipitation in terms of global mean whereas the DPT run properly reduces the overestimated precipitation amount along with a similar precipitation pattern (cf. Figs. 6b, c). In addition, the skill scores of the DPT run overall outperforms those from other runs (Table 2).

5. Summary and discussion

We investigate the impacts of the stochastic representation of model uncertainty, focusing particularly on the dynamical model tendency, which has not been attempted. A stochastic forcing that is dependent upon the forecast time and the height from the ground is designed using random number. The proposed method considers the preservation of the kinetic energy in the upper layer and the forecast skill's degradation of the deterministic model with the forecast time. A special attention has been given to the behavior of the stochastic representation in dynamic forcing on the fluctuations in model tendency and simulated climate, against what was in the traditional stochastic physics forcing.

Various sensitivity experiments are carried out to examine the sensitivity of fluctuations in the modeled tendency, to parameters in random forcing on deterministic medium-range

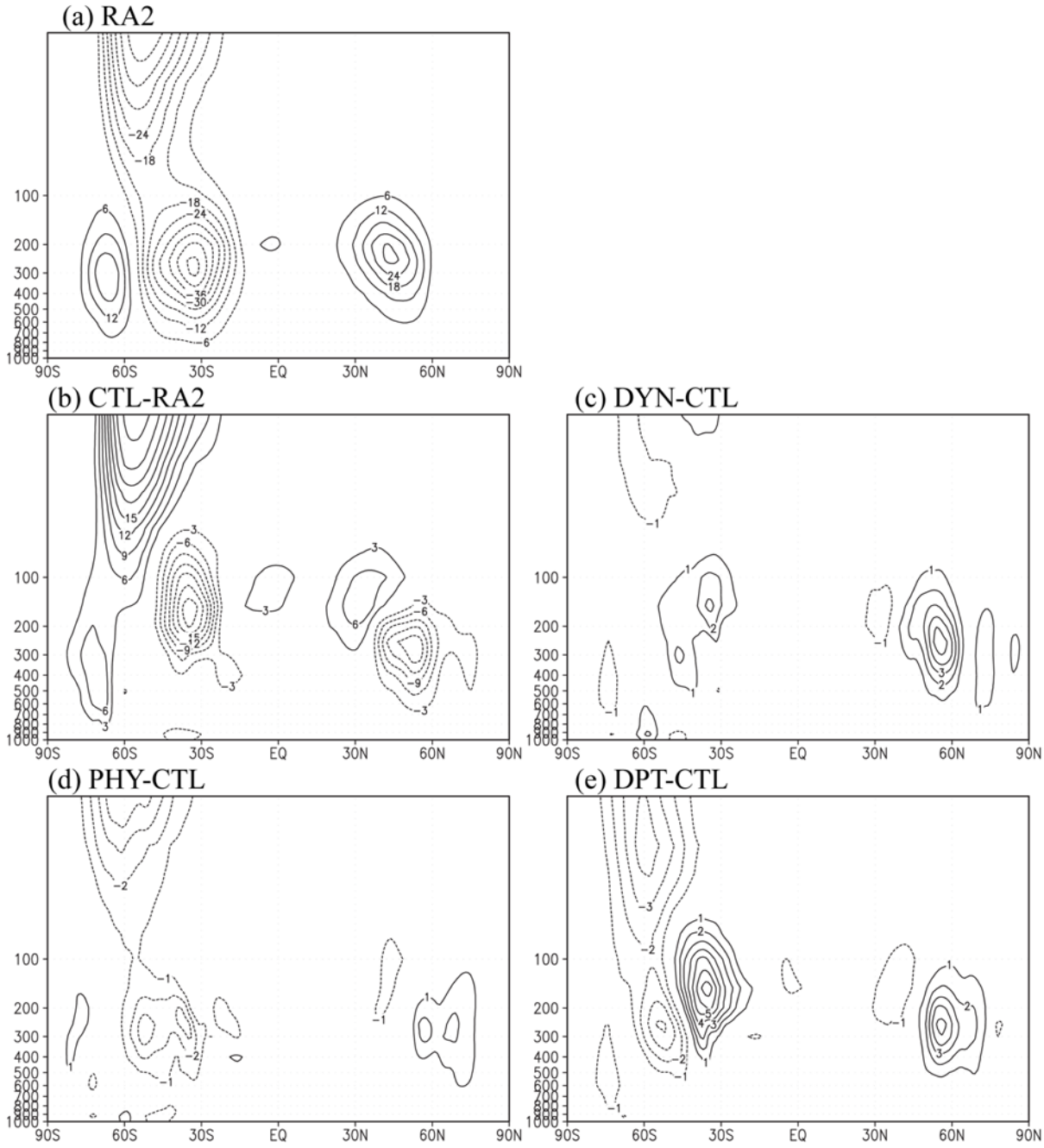

Fig. 5. (a) Transient eddy momentum flux ($u'v'$; $m^2\ s^{-2}$) obtained from the RA2 data and (b) the corresponding differences of (b) CTL minus RA2, (c) DYN minus CTL, (d) PHY minus CTL, and (e) DPT minus CTL, for a boreal summer of June-July-August in 1996. Contour intervals are 6, 3, and 1 for (a), (b), and (c-e), respectively.

forecast. Compared to the traditional approach of perturbing the physical tendency, the sensitivity of fluctuations in forecast variables to the magnitude of random forcing, is found to be greater in the case of perturbing the dynamical tendency. The linear increase of sensitivity in perturbing the dynamical tendency, to the magnitude of random forcing, is obtained, whereas the sensitivity is mixed when perturbation is applied to the physical tendency. Realizing that major advantage of the stochastic tendency in traditional approaches lies in the increase of ensemble spread, our approach sheds lights on the premise in ensemble prediction.

When both the dynamical and physical tendencies are simultaneously perturbed, an evaluation of seasonal ensemble prediction for a boreal summer in June-July-August (JJA) in 1996 demonstrates a significant enhancement in forecast skill in terms of poleward transient eddy and seasonal precipitation. This improvement of the forecast skill by perturbing both the physical and dynamical tendencies may be due to the fact that

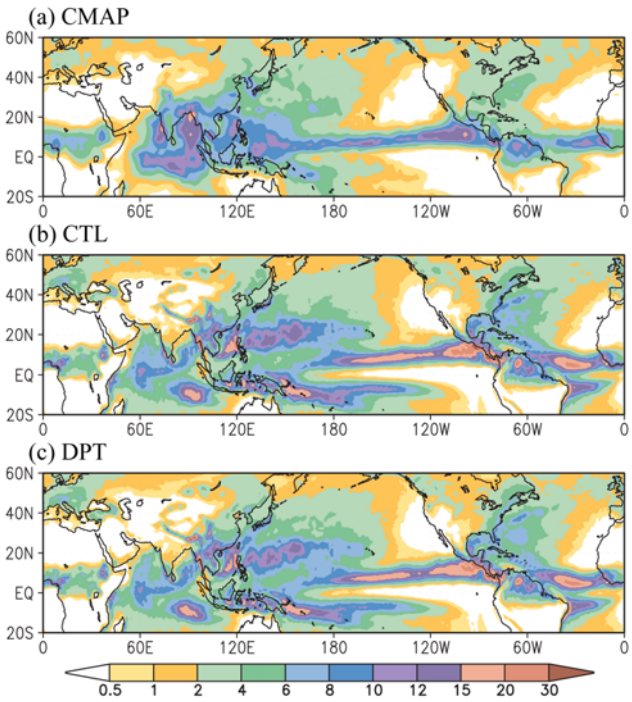

Fig. 6. Seasonal precipitation (mm d^{-1}) for a boreal summer of June-July-August in 1996, obtained from the (a) CMAP data and simulated from the (b) CTL and (c) DPT runs at a T126L64 resolution.

Table 2. Statistical verification scores for the globally-averaged precipitation amount (Ave.; mm d^{-1}) for a boreal summer of June-July-August in 1996. Boldface numbers designate the better performance.

Experiment	Ave.	Bias	RMSE	SC
CMAP	2.71	-	-	-
CTL	3.43	0.722	2.519	0.716
DYN	3.44	0.728	2.508	0.720
PHY	**3.48**	**0.767**	**2.592**	**0.707**
DPT	3.34	0.630	2.411	0.724

physical parameterizations also respond to the slightly perturbed dynamical state in order to preserve the consistency between the dynamics and physics (Berner *et al.*, 2009).

It is arguable that such a positive effect may apply only to the boreal summer of 1996, thus, we examined three more summers, as summarized in Table 3. The combined effect of perturbing physics and dynamics is so robust in 1998 summer as in 1996 summer, but not in 1997 and 1999 cases. It is however noted that even in 1997 and 1999 perturbing dynamics generally reveals a positive impact on the skill in the simulated large-scale and precipitation as compared to the experiment with the physics perturbation. A warm and cold El Niño-Southern Oscillation (ENSO) SST characteristics in 1997 and 1999 boreal summers, respectively, may influence the effect of the perturbed tendency, but further study is required.

Meanwhile, the application of 10-degree spatial correlation

Table 3. Skill scores of root-mean-square error (RMSE) and spatial correlation coefficient (SC) for standing eddy of the 500-hPa geopotential height (GPH; m) and precipitation (mm d^{-1}) for boreal summer (JJA) from 1997 to 1999. Boldface numbers designate the better performance.

	exp.	1997		1998		1999	
		RMSE	SC	RMSE	SC	RMSE	SC
GPH	CTL	22.06	0.787	25.05	0.520	23.93	0.679
	DYN	**21.18**	**0.806**	26.87	0.488	**20.33**	**0.782**
	PHY	23.86	0.756	26.96	0.497	21.45	0.751
	DPT	23.07	0.765	**24.42**	**0.559**	20.81	0.769
Precip.	CTL	2.59	0.707	2.70	0.691	2.70	0.687
	DYN	2.56	**0.713**	2.68	0.693	2.72	0.686
	PHY	2.60	0.712	2.80	0.679	2.76	0.684
	DPT	**2.53**	0.707	**2.55**	**0.696**	**2.55**	**0.696**

in random forcing, as in B1999, did increase the kinetic energy throughout the wavenumbers in the case of perturbing the dynamical tendency, which might be caused by the difference in the optimal spatial correlation scale between dynamics and physics. On the other hand, Gaussian or some other distributions for random sampling could bring further improvement in forecast skill. For a more robust evaluation of the proposed stochastic representation, we plan to evaluate the statistical skill in medium-range forecasts as well as seasonal simulations for extended period.

Acknowledgments. This work has been carried out through the R&D project on the development of global numerical weather prediction systems of Korea Institute of Atmospheric Prediction Systems (KIAPS) funded by Korea Meteorological Administration (KMA). The authors would like to acknowledge the support from KISTI supercomputing center through the strategic support program for the supercomputing application research [No. KSC-2013-G2-006].

Edited by: Jimy Dudhia

REFERENCES

Berner, J., T. Jung, and T. N. Palmer, 2012: Systematic model error: The impact of increased horizontal resolution versus improved stochastic and deterministic parameterizations. *J. Climate*, **25**, 4946-4962.

_____, G. J. Shutts, M. Leutbecher, and T. N. Palmer, 2009: A spectral stochastic kinetic energy backscatter scheme and its impact on flow-dependent predictability in the ECMWF ensemble prediction system. *J. Atmos. Sci.*, **66**, 603-626.

_____, S. Y. Ha, J. P. Hacker, A. Fournier, and C. Snyder, 2011: Model uncertainty in a mesoscale ensemble prediction system: Stochastic versus multiphysics representations. *Mon. Wea. Rev.*, **139**, 1972-1995.

Bishop, C. H., and K. T. Shanley, 2008: Bayesian model averaging's problematic treatment of extreme weather and a paradigm shift that fixes it. *Mon. Wea. Rev.*, **136**, 4641-4652.

Buizza, R., 2010: Horizontal resolution impact on short- and long-range forecast error. *Quart. J. Roy. Meteor. Soc.*, **136**, 1020-1035.

_____, M. Milleer, and T. N. Palmer, 1999: Stochastic representation of model uncertainties in the ECMWF ensemble prediction system. *Quart. J. Roy. Meteor. Soc.*, **125**, 2887-2908.

_____, P. L. Houtekamer, G. Pellerin, Z. Toth, Y. Zhu, and M. Wei, 2005: A comparison of the ECMWF, MSC, and NCEP global ensemble prediction systems. *Mon. Wea. Rev.*, **133**, 1076-1097.

Covey, C., K. M. AchutaRao, U. Cubasch, P. Jones, S. J. Lambert, M. E. Mann, T. J. Phillips, and K. E. Taylor, 2003: An overview of results from the coupled model intercomparison project. *Global Planet. Change*, **37**, 103-133.

Dai, A., 2006: Precipitation characteristics in eighteen coupled climate models. *J. Climate*, **19**, 4605-4630.

Dee, D. P., and Coauthors, 2011: The ERA-Interim reanalysis: Configuration and performance of the data assimilation system. *Quart. J. Roy. Meteor. Soc.*, **137**, 553-597.

Grell, G. A., and D. Dévényi, 2002: A generalized approach to parameterizing convection combining ensemble and data assimilation techniques. *Geophys. Res. Lett.*, **29**, 38-31-38-34.

Ham, S., and S.-Y. Hong, 2013: Sensitivity of simulated intraseasonal oscillation to four convective parameterization schemes in a coupled climate model. *Asia-Pac. J. Atmos. Sci.*, **49**, 483-496.

Hong, S.-Y., and J. Dudhia, 2012: Next-generation numerical weather prediction: Bridging parameterization, explicit clouds, and large eddies. *Bull. Amer. Meteor. Soc.*, **93**, ES6-ES9.

_____, M.-S. Koo, J. Jang, J.-E. Esther Kim, H. Park, M.-S. Joh, J.-H. Kang, and T.-J. Oh, 2013a: An evaluation of the software system dependency of a global atmospheric model. *Mon. Wea. Rev.*, **141**, 4165-4172.

_____, and Coauthors, 2013b: The Global/Regional Integrated Model system (GRIMs). *Asia-Pac. J. Atmos. Sci.*, **49**, 219-243.

Jung, T., T. N. Palmer, and G. J. Shutts, 2005: Influence of a stochastic parameterization on the frequency of occurrence of North Pacific weather regimes in the ECMWF model. *Geophys. Res. Lett.*, **32**, L23811.

Kanamitsu, M., W. Ebisuzaki, J. Woollen, S.-K. Yang, J. J. Hnilo, M. Fiorino, and G. L. Potter, 2002: NCEP-DOE AMIP-II Reanalysis (R-2). *Bull. Amer. Meteor. Soc.*, **83**, 1631-1643.

Kang, H.-S., and S.-Y. Hong, 2008: Sensitivity of the simulated East Asian summer monsoon climatology to four convective parameterization schemes. *J. Geophys. Res.*, **113**, D15119.

Krishnamurti, T. N., and J. Sanjay, 2003: A new approach to the cumulus parameterization issue. *Tellus A*, **55**, 275-300.

_____, K. Rajendran, T. S. V. Vijaya Kumar, S. Lord, Z. Toth, X. Zou, S. Cocke, J. E. Ahlquist, and I. M. Navon, 2003: Improved skill for the anomaly correlation of geopotential heights at 500 hPa. *Mon. Wea. Rev.*, **131**, 1082-1102.

LaRow, T. E., S. D. Cocke, and D. W. Shin, 2005: Multiconvective parameterizations as a multimodel proxy for seasonal climate studies. *J. Climate*, **18**, 2963-2978.

Lorenz, E. N., 1963: Deterministic nonperiodic flow. *J. Atmos. Sci.*, **20,** 130-141.

_____, 1969: The predictability of a flow which possesses many scales of motion. *Tellus*, **21**, 289-307.

_____, 1975: Climate predictability. *The physical basis of climate modelling WMO*, Geneva: World Meteorological Oragnization, 132-136.

Molteni, F., and T. N. Palmer, 1993: Predictability and finite-time instability of the northern winter circulation. *Quart. J. Roy. Meteor. Soc.*, **119**, 269-298.

Murphy, J. M., D. M. H. Sexton, D. N. Barnett, G. S. Jones, M. J. Webb, M. collins, and D. A. Stainforth, 2004: Quantification of modelling uncertainties in a large ensemble of climate change simulations. *Nature*, **430**.

Palmer, T. N., R. Buizza, F. J. Doblas-Reyes, T. Jung, M. Leutbecher, G. J. Shutts, M. Steinheimer, and A. Weisheimer, 2009: Stochastic parametrization and model uncertainty. Tech. Memo. 598, ECMWF, 42 pp.

Reynolds, R. W., and T. M. Smith, 1994: Improved global sea surface temperature analyses using optimum interpolation. *J. Climate*, **7**, 929-948.

Richardson, D. S., 2000: Skill and relative economic value of the ECMWF ensemble prediction system. *Quart. J. Roy. Meteor. Soc.*, **126**, 649-667.

Romps, D. M., 2012a: Weak pressure gradient approximation and its analytical solutions. *J. Atmos. Sci.*, **69**, 2835-2845.

_____, 2012b: Numerical tests of the weak pressure gradient approximation. *J. Atmos. Sci.*, **69**, 2846-2856.

Shutts, G., 2005: A kinetic energy backscatter algorithm for use in ensemble prediction systems. *Quart. J. Roy. Meteor. Soc.*, **131**, 3079-3102.

Stainforth, D. A., and Coauthors, 2005: Uncertainty in predictions of the climate response to rising levels of greehouse gases. *Nature*, **433**.

Tao, W.-K., D. Starr, A. Hou, P. Newman, and Y. Sud, 2003: A cumulus parameterization workshop. *Bull. Amer. Meteor. Soc.*, **84**, 1055-1062.

Teixeira, J., C. A. Reynolds, and K. Judd, 2007: Time step sensitivity of nonlinear atmospheric models: Numerical convergence, truncation error growth, and ensemble design. *J. Atmos. Sci.*, **64**, 175-189.

Weigel, A. P., M. A. Liniger, and C. Appenzeller, 2008: Can multi-model combination really enhance the prediction skill of probabilistic ensemble forecasts?. *Quart. J. Roy. Meteor. Soc.*, **134**, 241-260.

Weisheimer, A., T. N. Palmer, and F. J. Doblas-Reyes, 2011: Assessment of representations of model uncertainty in monthly and seasonal forecast ensembles. *Geophys. Res. Lett.*, **38**, L16703.

Xie, P., and P. A. Arkin, 1997: Global precipitation: A 17-year monthly analysis based on gauge observations, satellite estimates, and numerical model outputs. *Bull. Amer. Meteor. Soc.*, **78**, 2539-2558.